

1 Title: Population clustering of structural brain aging and its association with 2 brain development

3

4 **Authors:** Haojing Duan^{1,2}, Runye Shi³, Jujiao Kang^{1,2}, Tobias Banaschewski⁴, Arun L. W.
5 Bokde⁵, Christian Büchel⁶, Sylvane Desrivieres⁷, Herta Flor^{8,9}, Antoine Grigis¹⁰, Hugh
6 Garavan¹¹, Penny A. Gowland¹², Andreas Heinz¹³, Rüdiger Brühl¹⁴, Jean-Luc Martinot¹⁵,
7 Marie-Laure Paillère Martinot¹⁶, Eric Artiges¹⁷, Frauke Nees^{4,8,18}, Dimitri Papadopoulos
8 Orfanos¹⁰, Tomáš Paus^{19,20}, Luise Poustka²¹, Sarah Hohmann⁴, Nathalie Holz⁴, Juliane H.
9 Fröhner²², Michael N. Smolka²², Nilakshi Vaidya²³, Henrik Walter¹³, Robert Whelan²⁴,
10 Gunter Schumann^{1,23,25,26}, Xiaolei Lin^{3,27*}, Jianfeng Feng^{1,2,3,28,29*}, IMAGEN consortium

11 Affiliations:

12 ¹ Institute of Science and Technology for Brain-Inspired Intelligence, Fudan University, Shanghai, China

13 ² Key Laboratory of Computational Neuroscience and Brain-Inspired Intelligence (Fudan University),
14 Ministry of Education, China

15 ³ School of Data Science, Fudan University, Shanghai, China

16 ⁴ Department of Child and Adolescent Psychiatry and Psychotherapy, Central Institute of Mental Health,
17 Medical Faculty Mannheim, Heidelberg University, Square J5, 68159 Mannheim, Germany

18 ⁵ Discipline of Psychiatry, School of Medicine and Trinity College Institute of Neuroscience, Trinity
19 College Dublin, Dublin, Ireland

20 ⁶ University Medical Centre Hamburg-Eppendorf, Hamburg, Germany

21 ⁷ Social Genetic and Developmental Psychiatry Centre, Institute of Psychiatry, Psychology and
22 Neuroscience, King's College London, London, UK

23 ⁸ Institute of Cognitive and Clinical Neuroscience, Central Institute of Mental Health, Medical Faculty
24 Mannheim, Heidelberg University, Square J5, Mannheim, Germany

25 ⁹ Department of Psychology, School of Social Sciences, University of Mannheim, 68131 Mannheim,
26 Germany

27 ¹⁰ NeuroSpin, CEA, Université Paris-Saclay, F-91191 Gif-sur-Yvette, France

28 ¹¹ Departments of Psychiatry and Psychology, University of Vermont, 05405 Burlington, Vermont, USA

29 ¹² Sir Peter Mansfield Imaging Centre School of Physics and Astronomy, University of Nottingham,
30 University Park, Nottingham, United Kingdom

31 ¹³ Department of Psychiatry and Psychotherapy CCM, Charité – Universitätsmedizin Berlin, corporate
32 member of Freie Universität Berlin, Humboldt-Universität zu Berlin, and Berlin Institute of Health, Berlin,
33 Germany

34 ¹⁴ Physikalisch-Technische Bundesanstalt (PTB), Braunschweig and Berlin, Germany

35 ¹⁵ Institut National de la Santé et de la Recherche Médicale, INSERM U A10 "Trajectoires
36 développementales en psychiatrie"; Université Paris-Saclay, Ecole Normale supérieure Paris-Saclay,
37 CNRS, Centre Borelli; Gif-sur-Yvette, France

38 ¹⁶ Institut National de la Santé et de la Recherche Médicale, INSERM U A10 "Trajectoires
39 développementales & psychiatrie", University Paris-Saclay, Ecole Normale Supérieure Paris-Saclay,
40 CNRS; Centre Borelli, Gif-sur-Yvette, France; and AP-HP. Sorbonne Université, Department of Child and
41 Adolescent Psychiatry, Pitié-Salpêtrière Hospital, Paris, France

42 ¹⁷ Institut National de la Santé et de la Recherche Médicale, INSERM U A10 "Trajectoires

43 **NOTE:** This preprint reports new research that has not been certified by peer review and should not be used to guide clinical practice.
développementales en psychiatrie"; Université Paris-Saclay, Ecole Normale supérieure Paris-Saclay,

44 CNRS, Centre Borelli, Gif-sur-Yvette; and Psychiatry Department, EPS Barthélemy Durand, Etampes,
45 France
46 ¹⁸ Institute of Medical Psychology and Medical Sociology, University Medical Center Schleswig-Holstein
47 Kiel University, Kiel, Germany
48 ¹⁹ Department of Psychiatry, Faculty of Medicine and Centre Hospitalier Universitaire Sainte-Justine,
49 University of Montreal, Montreal, Quebec, Canada
50 ²⁰ Departments of Psychiatry and Psychology, University of Toronto, Toronto, Ontario, Canada
51 ²¹ Department of Child and Adolescent Psychiatry and Psychotherapy, University Medical Centre
52 Göttingen, von-Siebold-Str. 5, 37075, Göttingen, Germany
53 ²² Department of Psychiatry and Neuroimaging Center, Technische Universität Dresden, Dresden,
54 Germany
55 ²³ Department of Psychiatry and Neurosciences, Charité–Universitätsmedizin Berlin, corporate member of
56 Freie Universität Berlin/Humboldt-Universität zu Berlin, and Berlin Institute of Health, Berlin, Germany
57 ²⁴ School of Psychology and Global Brain Health Institute, Trinity College Dublin, Ireland
58 ²⁵ Centre for Population Neuroscience and Stratified Medicine (PONS Centre), ISTBI, Fudan University,
59 Shanghai, China
60 ²⁶ Centre for Population Neuroscience and Stratified Medicine (PONS), Department of Psychiatry and
61 Psychotherapy, Charité Universitätsmedizin Berlin, Germany
62 ²⁷ Huashan Institute of Medicine, Huashan Hospital affiliated to Fudan University, Shanghai, China
63 ²⁸ MOE Frontiers Center for Brain Science, Fudan University, Shanghai, China
64 ²⁹ Zhangjiang Fudan International Innovation Center, Shanghai, China
65
66 * Correspondence authors.
67 Xiaolei Lin (Address: School of Data Science, Fudan University, Shanghai, 200433, China. Email:
68 xiaoleilin@fudan.edu.cn)
69 or
70 Jianfeng Feng (Address: Institute of Science and Technology for Brain-inspired Intelligence, Fudan
71 University, Shanghai, 200433, China. Email: jianfeng64@gmail.com)

72 **Abstract**

73 Structural brain aging has demonstrated strong inter-individual heterogeneity and mirroring
74 patterns with brain development. However, due to the lack of large-scale longitudinal
75 neuroimaging studies, most of the existing research focused on the cross-sectional changes of
76 brain aging. In this investigation, we present a data-driven approach that incorporate both cross-
77 sectional changes and longitudinal trajectories of structural brain aging and identified two brain
78 aging patterns among 37,013 healthy participants from UK Biobank. Participants with
79 accelerated brain aging also demonstrated accelerated biological aging, cognitive decline and
80 increased genetic susceptibilities to major neuropsychiatric disorders. Further, by integrating
81 longitudinal neuroimaging studies from a multi-center adolescent cohort, we validated the “last
82 in, first out” mirroring hypothesis and identified brain regions with manifested mirroring
83 patterns between brain aging and brain development. Genomic analyses revealed risk loci and
84 genes contributing to accelerated brain aging and delayed brain development, providing
85 molecular basis for elucidating the biological mechanisms underlying brain aging and related
86 disorders.

87 **Introduction**

88 The structure of the brain undergoes continual changes throughout the entire lifespan, with
89 structural brain alterations intimately linking brain development and brain aging^{1,2}. Brain aging
90 is a progressive process that often co-occurs with biological aging and declines of cognitive
91 functions³⁻⁵, which contribute to the onset and acceleration of neurodegenerative⁶ and
92 neuropsychiatric disorders⁷. Studies on healthy brain aging have revealed significant inter-
93 individual heterogeneity in the patterns of neuroanatomical changes^{8,9}. Therefore, examining
94 the patterns of structural brain aging and its associations with cognitive decline is of paramount
95 importance in understanding the diverse biological mechanisms of age-related
96 neuropsychiatric disorders.

97 Despite the fact that there exist large differences between brain development and brain
98 aging¹⁰, a discernible association between these two processes remains evident. Direct
99 comparisons of brain development and brain aging using structural MRI indicated a “last in,
100 first out” mirroring pattern, where brain regions develop relatively late during adolescence
101 demonstrated accelerated degeneration in older ages^{11,12}. In addition, brain regions with strong
102 mirroring effects showed increased vulnerability to neurodegenerative and neuropsychiatric
103 disorders, including Alzheimer’s disease and schizophrenia¹³. However, due to the lack of
104 large-scale longitudinal MRI studies during adolescence and mid-to-late adulthood, validation
105 of the “last in, first out” mirroring hypothesis remains unavailable.

106 Prior investigations have largely focused on regional and cross-sectional changes of brain
107 aging^{9,13,14}, with relatively few studies exploring longitudinal trajectories of brain aging and its
108 associations with brain development^{8,15,16}. In this article, we present a data-driven approach to
109 examine the population clustering of longitudinal brain aging trajectories using structure MRI
110 data obtained from 37,013 healthy individuals during mid-to-late adulthood (44-82 years), and
111 explore its association with biological aging, cognitive decline and susceptibilities for
112 neuropsychiatric disorders. Further, mirroring patterns between longitudinal brain
113 development and brain aging are investigated by comparing the region-specific aging /
114 developmental trajectories, and manifestation of the mirroring patterns are investigated across
115 the whole-brain and among participants with different brain aging patterns. Genomic analyses

116 are conducted to reveal risk loci and genes associated with accelerated brain aging and delayed
117 brain development.

118

119 **Results**

120 **Longitudinal trajectories of whole-brain GMV in mid-to-late adulthood define two brain** 121 **aging patterns.**

122 Fig. 1 provides the data sources, analytical workflow and research methodology of this study.
123 Longitudinal GMV trajectories in 40 ROIs (33 cortical and 7 subcortical ROIs) were estimated
124 for each of the 37,013 healthy participants in UK Biobank. After dimension reduction via
125 principal component analysis, the first 15 principal components (PCs) were used in the
126 clustering analysis (see Methods)^{17,18}. Two brain aging patterns were identified, where 18,929
127 (51.1%) participants with the first brain aging pattern (pattern 1) had higher total GMV at
128 baseline and a slower rate of GMV decrease over time, and the remaining participants with the
129 second pattern (pattern 2) had lower total GMV at baseline and a faster rate of GMV decrease
130 (Fig. 2a). Comparing the region-specific rate of GMV decrease, pattern 2 showed a more rapid
131 GMV decrease in medial occipital (lingual gyrus, cuneus and pericalcarine cortex) and medial
132 temporal (entorhinal cortex, parahippocampal gyrus) regions (Fig. 2b, c and Supplementary
133 Fig. 3), which had the largest loadings in the second and third principal components
134 (Supplementary Table 5). Sample characteristics of these 37,013 UK Biobank participants
135 stratified by brain aging patterns are summarized in Supplementary Table 6. Overall,
136 participants with different brain aging patterns had similar distributions with regard to age, sex,
137 ethnicity, smoking status, Townsend Deprivation Index, BMI and years of schooling.

138

139 **Brain aging patterns were significantly associated with biological aging.**

140 To explore the relationships between structural brain aging and biological aging, we
141 investigated the distribution of aging biomarkers, such as telomere length and PhenoAge¹⁹,
142 across brain aging patterns identified above (Fig. 3 and Supplementary Table 7). Compared to
143 pattern 1, participants in pattern 2 with more rapid GMV decrease had shorter leucocyte
144 telomere length ($P = 0.009$, Cohen's $D = -0.028$) and this association remained consistent after

145 adjusting for sex, age, ethnic, BMI, smoking status and alcohol intake frequency²⁰. Next, we
146 examined PhenoAge, which was developed as an aging biomarker incorporating composite
147 clinical and biochemical data¹⁹, and observed higher PhenoAge among participants with brain
148 aging pattern 2 compared to pattern 1 ($P = 0.019$, Cohen's $D = 0.027$). Again, the association
149 remained significant after adjusting for sex, age, ethnic, BMI, smoking status, alcohol intake
150 frequency and education years ($P = 3.05 \times 10^{-15}$, Cohen's $D = 0.092$). **Group differences in**
151 **terms of each individual component of PhenoAge (including albumin, creatinine, glucose, c-**
152 **reactive protein, lymphocytes percentage, mean corpuscular volume, erythrocyte distribution**
153 **width, alkaline phosphatase and leukocyte count) were also investigated and results were**
154 **consistent with PhenoAge (Supplementary Fig. 4).**

155

156 **Accelerated brain aging was associated with cognitive decline and increased genetic** 157 **susceptibilities to ADHD and delayed brain development.**

158 Next, we conducted comprehensive comparisons of cognitive functions between participants
159 with different brain aging patterns. In general, those with brain aging pattern 2 (lower baseline
160 total GMV and more rapid GMV decrease) exhibited worse cognitive performances compared
161 to pattern 1. Specifically, brain aging pattern 2 showed lower numbers of correct pairs matching
162 ($P = 0.006$, Cohen's $D = -0.029$), worse prospective memory (OR = 0.943, 95% CI [0.891,
163 0.999]), lower fluid intelligence ($P < 1.00 \times 10^{-20}$, Cohen's $D = -0.102$), and worse numeric
164 memory ($P = 5.97 \times 10^{-11}$, Cohen's $D = -0.082$). No statistically significant differences were
165 observed in terms of the reaction time ($P = 0.99$) and prospective memory ($P = 0.052$) between
166 these two brain aging patterns after FDR correction. Results were consistent when using
167 models adjusted for sex, age, and socioeconomic status (TDI, education and income)^{21,22} (Fig.
168 4). Full results demonstrating the associations between brain aging patterns and cognitive
169 functions are presented in Supplementary Table 8.

170 **Having observed cognitive decline among participants with accelerated brain aging pattern, we**
171 **next investigated whether brain aging patterns were associated with genetic vulnerability to**
172 **major neuropsychiatric disorders. Since current GWAS are under-powered for ADHD and ASD**
173 **and the difficulty in identifying genetic variants was likely due to their polygenic nature, we**

174 calculated the corresponding polygenic risk scores (PRS) using multiple p value thresholds.
175 This approach enabled robust investigation of the association between genetic susceptibility of
176 neuropsychiatric disorders and brain imaging phenotypes. PRS for major neuro-developmental
177 disorders including attention-deficit/hyperactivity disorder (ADHD) and autism spectrum
178 disorders (ASD), neurodegenerative diseases including Alzheimer's disease (AD) and
179 Parkinson's disease (PD), neuropsychiatric disorders including bipolar disorder (BIP), major
180 depressive disorder (MDD), and schizophrenia (SCZ), and delayed structural brain
181 development (GWAS from an unpublished longitudinal neuroimaging study)²³ were calculated
182 for each participant using multiple P value thresholds (from 0.005 to 0.5 at intervals of 0.005)
183 and results were then averaged over all thresholds (Fig. 5). Overall, we observed increased
184 genetic susceptibility to ADHD ($P = 0.040$) and delayed brain development ($P = 1.48 \times 10^{-6}$)
185 among participants with brain aging pattern 2 after FDR correction, while no statistically
186 significant differences were observed for ASD, AD, PD, BIP, MDD and SCZ (Fig. 5). Details
187 regarding the genetic liability to other common diseases and phenotypes using enhanced PRS
188 from UK Biobank are displayed in Supplementary Table 10 and 11.

189

190 **Genome Wide Association Studies (GWAS) identified significant genetic loci associated** 191 **with accelerated brain aging.**

192 Having observed significant associations between brain aging patterns and cognitive
193 performances / genetic liabilities to major neurodevelopmental disorders, we further
194 investigated if there exist genetic variants contributing to individualized brain aging phenotype.
195 We conducted genome-wide association studies (GWAS) using estimated total GMV at 60
196 years old as the phenotype. This phenotype was derived by adding individual specific
197 deviations to the population averaged total GMV, thus providing additional information
198 compared to studies using only cross-sectional neuroimaging phenotypes.

199 Six independent single nucleotide polymorphisms (SNPs) were identified at genome-wide
200 significance level ($P < 5 \times 10^{-8}$) (Fig. 6) and were subsequently mapped to genes using NCBI,
201 Ensembl and UCSC Genome Browser database (Supplementary Table 12). Among them, two
202 SNPs (rs10835187 and rs779233904) were also found to be associated with multiple brain

203 imaging phenotypes in previous studies²⁴. Compared to the GWAS using global gray matter
204 volume as the phenotype, our GWAS revealed additional signal in chromosome 7 (rs7776725),
205 which was mapped to the intron of FAM3C and encodes a secreted protein involved in
206 pancreatic cancer²⁵ and Alzheimer's disease²⁶. This signal was further validated to be associated
207 with specific brain aging mode by another study using a data-driven decomposition approach²⁷.
208 In addition, another significant loci (rs10835187, $P = 1.11 \times 10^{-13}$) is an intergenic variant
209 between gene LGR4-AS1 and LIN7C, and was reported to be associated with bone density and
210 brain volume measurement^{24,28}. *LIN7C* encodes the Lin-7C protein, which is involved in the
211 localization and stabilization of ion channels in polarized cells, such as neurons and epithelial
212 cells^{29,30}. Previous study has revealed the association of both allelic and haplotypic variations
213 in the *LIN7C* gene with ADHD³¹.

214

215 **Mirroring patterns between brain aging and brain development.**

216 Having observed significant associations between brain aging and genetic susceptibility to
217 neurodevelopmental disorders, we are now interested in examining the mirroring patterns
218 between brain aging and brain development in the whole population, and whether these
219 mirroring patterns were more pronounced in those with accelerated brain aging. Adolescents
220 in the IMAGEN cohort showed more rapid GMV decrease in the frontal and parietal lobes,
221 especially the frontal pole, superior frontal gyrus, rostral middle frontal gyrus, inferior parietal
222 lobule and superior parietal lobule, while those in their mid-to-late adulthood showed more
223 accelerated GMV decrease in the temporal lobe, including medial orbitofrontal cortex, inferior
224 parietal lobule and lateral occipital sulcus (Fig. 7a). The mirroring patterns (with slower GMV
225 decrease during brain development and more rapid GMV decrease during brain aging) were
226 particularly prominent in inferior temporal gyrus, caudal anterior cingulate cortex, fusiform
227 cortex, middle temporal gyrus and rostral anterior cingulate cortex (Fig. 7b). The regional
228 mirroring patterns became weaker when we focus on late brain aging at age 75 years old,
229 especially in the frontal lobe and cingulate cortex. Further, mirroring patterns were represented
230 more prominently in participants with brain aging pattern 2, where stronger mirroring between

231 brain aging and brain development was observed in frontotemporal area, including lateral
232 occipital sulcus and lingual gyrus (Fig. 7c).

233

234 **Gene expression profiles were associated with delayed brain development and accelerated**
235 **brain aging.**

236 The Allen Human Brain Atlas (AHBA) transcriptomic dataset (<http://human.brain-map.org>)
237 were used to obtain the spatial correlation between whole-brain gene expression profiles and
238 structural brain development/aging via partial least square (PLS) regression. The first PLS
239 component explained 24.7% and 53.6% of the GMV change during brain development
240 (estimated at age 15y, $r_{\text{spearman}} = 0.51$, $P_{\text{permutation}} = 0.03$) and brain aging (estimated at age 55y,
241 $r_{\text{spearman}} = 0.49$, $P_{\text{permutation}} < 0.001$), respectively. Seventeen of the 45 genes mapped to GWAS
242 significant SNP were found in AHBA, with *LGR4* ($r_{\text{spearman}} = 0.56$, $P_{\text{permutation}} < 0.001$)
243 significantly associated with delayed brain development and *ESR1* ($r_{\text{spearman}} = 0.53$, $P_{\text{permutation}} <$
244 0.001) and *FAM3C* ($r_{\text{spearman}} = -0.37$, $P_{\text{permutation}} = 0.004$) significantly associated with
245 accelerated brain aging. *BDNF-AS* was positively associated with both delayed brain
246 development and accelerated brain aging after spatial permutation test (Supplementary Table
247 13 and 14).

248 Next, we screened the genes based on their contributions and effect directions to the first
249 PLS components in brain development and brain aging. 990 and 2293 genes were identified to
250 be positively associated with brain development and negatively associated with brain aging at
251 FDR corrected P value of 0.05, respectively, representing gene expressions associated with
252 delayed brain development and accelerated brain aging. These genes were then tested for
253 enrichment of GO biological processes and KEGG pathways. Genes associated with delayed
254 brain development showed significant enrichment in “regulation of trans-synaptic signaling”,
255 “forebrain development”, “signal release” and “cAMP signaling pathway” (Fig. 8a), and genes
256 associated with accelerated brain aging showed significant enrichment in “macroautophagy”,
257 “establishment of protein localization to organelle”, “histone modification”, and “pathways of
258 neurodegeneration – multiple diseases” (Fig. 8b). Full results of the gene set enrichment
259 analysis were provided in Supplementary Fig. 5.

260

261 **Discussion**

262 In this study, we adopted a data-driven approach and revealed two distinct brain aging patterns
263 using large-scale longitudinal neuroimaging data in mid-to-late adulthood. Compared to brain
264 aging pattern 1, brain aging pattern 2 were characterized by a faster rate of GMV decrease,
265 accelerated biological aging, cognitive decline, and genetic susceptibility to
266 neurodevelopmental disorders. By integrating longitudinal neuroimaging data from adult and
267 adolescent cohorts, we demonstrated the “last in, first out” mirroring patterns between
268 structural brain aging and brain development, and showed that the mirroring pattern was
269 manifested in the temporal lobe and among participants with accelerated brain aging. Further,
270 genome-wide association studies identified significant genetic loci contributing to accelerated
271 brain aging, while spatial correlation between whole-brain transcriptomic profiles and
272 structural brain aging / development revealed important gene sets associated with both
273 accelerated brain aging and delayed brain development.

274 Brain aging is closely related to the onset and progression of neurodegenerative and
275 neuropsychiatric disorders. Both neurodegenerative and neuropsychiatric disorders
276 demonstrate strong inter-individual heterogeneity, which prevents the comprehensive
277 understanding of their neuropathology and neurogenetic basis. Therefore, multidimensional
278 investigation into disease subtyping and population clustering of structural brain aging are
279 crucial in elucidating the sources of heterogeneity and neurophysiological basis related to the
280 disease spectrum³². In the last decades, major developments in the subtyping of Alzheimer's
281 disease, dementia and Parkinson's disease, have provided new perspectives regarding their
282 clinical diagnosis, treatment, disease progression and prognostics³²⁻³⁴. While previous studies
283 of brain aging mostly focused on the cross-sectional differences between cases and healthy
284 controls, we here delineated the structural brain aging patterns among healthy participants
285 using a novel data-driven approach that captured both cross-sectional and longitudinal
286 trajectories of the whole-brain gray matter volume^{35,36}. The two brain aging patterns identified
287 using the above approach showed large differences in the rate of change in medial
288 occipitotemporal gyrus, which is involved in vision, word processing and scene recognition³⁷⁻

289 ³⁹. Significant reduction of the gray matter volume and abnormal changes of the functional
290 connectivity in this region were found in subjects with mild cognitive impairment (MCI) and
291 AD, respectively^{40,41}. Consistent with previous research, participants with accelerated brain
292 aging pattern also exhibited accelerated biological aging and poor levels of cognitive
293 performance²⁴. Our results support the establishment of a network connecting brain aging
294 patterns with biological aging profiles involving multi-organ systems throughout the body⁴².
295 Since structural brain patterns might manifest and diverge decades before cognitive decline⁴³,
296 subtyping of brain aging patterns could aid in the early prediction of cognitive decline and
297 severe neurodegenerative and neuropsychiatric disorders.

298 Mirroring pattern between brain development and brain aging has long been hypothesized
299 by postulating that phylogenetically newer and ontogenetically less precocious brain structures
300 degenerate relatively early¹³. Early studies have reported a positive correlation between age-
301 related differences of cortical volumes and precedence of myelination of intracortical fibers⁴⁴.
302 Here, we compared the annual volume change of the whole-brain gray matter during brain
303 development and early / late stages of brain aging, and found that mirroring patterns are
304 predominantly localized to the lateral / medial temporal cortex and the cingulate cortex, which
305 is consistent with previous findings¹². These cortical regions characterized by “last-in, first-out”
306 mirroring patterns showed increased vulnerability to the several neuropsychiatric disorders.
307 For example, regional deficits in the superior temporal gyrus and medial temporal lobe were
308 observed in schizophrenia⁴⁵, along with morphological abnormalities in the medial
309 occipitotemporal gyrus⁴⁶. Children diagnosed with ADHD had lower brain surface area in the
310 frontal, cingulate, and temporal regions⁴⁷. Douaud et al.¹³ revealed a population transmodal
311 network with lifespan trajectories characterized by the mirroring pattern of development and
312 aging. We investigated the genetic susceptibility to individual-level mirroring patterns based
313 on the lasting impact of neurodevelopmental genetic factors on brain¹⁵, demonstrating that
314 those with more rapidly brain aging patterns have a higher risk of delayed development.

315 Identifying genes contributing to structural brain aging remains a critical step in
316 understanding the molecular changes and biological mechanisms that govern age-related
317 cognitive decline. Several genetic loci have been reported to be associated with brain aging

318 modes and neurocognitive decline, many of which demonstrated global overlap with
319 neuropsychiatric disorders and their related risk factors^{27,48,49}. Here, we focused on the
320 individual brain aging phenotype by estimating individual deviation from the population
321 averaged total GMV and conducted genome-wide association analysis with this phenotype.
322 Our approach identified 6 risk SNPs associated with accelerated brain aging, most of which
323 could be further validated by previous studies using population averaged brain aging
324 phenotypes. However, our approach revealed additional genetic signals and demonstrated
325 genetic architecture underlying brain aging patterns overlap with bone density^{28,50}. In addition,
326 molecular profiling of the aging brain has been thoroughly investigated among patients with
327 neurodegenerative diseases, but rarely conducted to shed light on the mirroring patterns among
328 healthy participants. Analysis of the spatial correlation between gene expression profiles and
329 structural brain development / aging further identified genes contributing to delayed brain
330 development and accelerated brain aging. Specifically, expression of gene *BDNF-AS* was
331 significantly associated with both processes. *BDNF-AS* is an antisense RNA gene and plays a
332 role in the pathoetiology of non-neoplastic conditions mainly through the mediation of *BDNF*⁵¹.
333 *LGR4* (associated with delayed brain development) and *FAM3C* (associated with accelerated
334 brain aging) identified in the spatial genetic association analysis also validated our findings in
335 the GWAS.

336 There are several limitations in the current study that need to be addressed in future research.
337 Firstly, the UK Biobank cohort, which we leveraged to identify population clustering of brain
338 aging patterns, had a limited number of repeated structural MRI scans. Therefore, it remains
339 challenging to obtain robust estimation of the longitudinal whole-brain GMV trajectory at the
340 individual level. As a robustness check, we have calculated both intra-class correlation and
341 variance of both random intercept and age slope to ensure appropriateness of the mixed effect
342 models. Secondly, although aging is driven by numerous hallmarks, we have only investigated
343 the association between brain aging patterns and biological aging in terms of telomere length
344 and blood biochemical markers due to limitations of data access. Other dimensions of aging
345 hallmarks and their relationship with structural brain aging need to be investigated in the future.
346 Thirdly, our genomic analyses were restricted to "white British" participants of European

347 ancestry. The diversity of genomic analyses will continue to improve as the sample sizes of
348 GWAS of non-European ancestry increase. Further, although the gene expression maps from
349 Allen Human Brain Atlas enabled us to gain insights into the spatial coupling between gene
350 expression profiles and mirroring patterns of the brain, the strong inter-individual variation of
351 whole-brain gene expression levels and large temporal span of the human brain samples may
352 lead to the inaccurate correspondence in the observed associations. Finally, we focused on
353 structural MRIs in deriving brain aging patterns in this analysis, future investigations could
354 consider other brain imaging modalities from a multi-dimensional perspective. Nevertheless,
355 our study represents a novel attempt for population clustering of structural brain aging and
356 validated the mirroring pattern hypothesis by leveraging large-scale adolescent and adult
357 cohorts.

358 **Methods**

359 **Participants** T1-weighted brain MRI images were obtained from 37,013 individuals aged 44-
360 82 years old from UK Biobank (36,914 participants at baseline visit in 2014+, 4,007
361 participants at the first follow-up visit in 2019+). All participants provided written informed
362 consent, and ethical approval was granted by the North West Multi-Center Ethics committee
363 (<https://www.ukbiobank.ac.uk/learn-more-about-uk-biobank/about-us/ethics>). Participants
364 were excluded if they were diagnosed with severe psychiatric disorders or neurological
365 diseases using ICD-10 primary and secondary diagnostic codes or from self-reported medical
366 conditions at UK Biobank assessment center (see Supplementary Tables 1 and 2). Data were
367 obtained under application number 19542. 1,529 adolescents with structural MRI images were
368 drawn from the longitudinal project IMAGEN (1,463 at age 14, 1,377 at age 19 and 1,148 at
369 age 23), of which the average number of MRI scans was 2.61 per adolescent. The IMAGEN
370 study was approved by local ethics research committees at each research site and informed
371 consent was given by all participants and a parent/guardian of each participant. Workflow for
372 participant selection is illustrated in Supplementary Fig. 1.

373
374 **MRI acquisition** Quality-controlled T1-weighted neuroimaging data from UK Biobank and
375 IMAGEN were processed using FreeSurfer v6.0. Detailed imaging processing pipeline can be
376 found online for UK Biobank (https://biobank.ctsu.ox.ac.uk/crystal/crystal/docs/brain_mri.pdf)
377 and IMAGEN (https://github.com/imagen2/imagen_mri). Briefly, cortical gray matter volume
378 (GMV) from 33 regions in each hemisphere were generated using Desikan–Killiany Atlas⁵²,
379 and total gray matter volume (TGMV), intracranial volume (ICV) and subcortical volume were
380 derived from ASEG atlas⁵³ (See Supplementary Table 3). Regional volume was averaged
381 across left and right hemispheres. To avoid deficient segmentation or parcellation, participants
382 with TGMV, ICV or regional GMV beyond 4 standard deviations from the sample mean were
383 considered as outliers and removed from the following analyses.

384
385 **Identification of longitudinal brain aging patterns** Whole-brain GMV trajectory was
386 estimated for each participant in 40 brain regions of interest (ROIs) (33 cortical regions and 7

387 subcortical regions), using mixed effect regression model with fixed linear and quadratic age
388 effects, random intercept and random age slope. Covariates include sex, assessment center,
389 handedness, ethnic, and ICV. Models with random intercept and with both random intercept
390 and random age slope were compared using AIC, BIC and evaluation of intra-class correlation
391 (ICC). Results suggested that random age slope model should be chosen for almost all ROIs
392 (Supplementary Table 4). Deviation of regional GMV from the population average was
393 calculated for each participant at age 60 years and dimension reduction was conducted via
394 Principal Component Analysis. The first 15 principal components explaining approximately
395 70% of the total variations of regional GMV deviation were used in multivariate k-means
396 clustering. Optimal number of clusters was chosen using both elbow diagram and contour
397 coefficient (Supplementary Fig. 2). Rates of volumetric change for total gray matter and each
398 ROI were estimated using generalized additive mixed effect models (GAMM) with fixed cubic
399 splines of age, random intercept and random age slope, which incorporates both cross-sectional
400 between-subject variation and longitudinal within-subject variation from 40,921 observations
401 and 37,013 participants. Covariates include sex, assessment center, handedness, ethnic, and
402 ICV.

403

404 **Association between brain aging patterns and biological aging, cognitive decline and**
405 **genetic susceptibilities of neuropsychiatric disorders** Individuals with Z-standardized
406 leucocyte telomere length⁵⁴ and blood biochemistry (which were used to calculate PhenoAge¹⁹
407 that characterizes biological aging) outside 4 standard deviations from the sample mean were
408 excluded for better quality control. A total of 11 cognitive tests performed on the touchscreen
409 questionnaire were included in the analysis. More information about the cognitive tests is
410 provided in Supplementary Information. Comparisons of biological aging (leucocyte telomere
411 length, PhenoAge) and cognitive function were conducted among participants with different
412 brain aging patterns using both unadjusted and adjusted multivariate regression models with
413 Bonferroni / FDR correction. Polygenic Risk Scores (PRS) were calculated for autism spectrum
414 disorder (ASD), attention deficit hyperactivity disorder (ADHD), Alzheimer's disease (AD),
415 Parkinson's Disease (PD), bipolar disorder (BIP), major depressive disorder (MDD),

416 schizophrenia (SCZ) and delayed brain development using GWAS summary statistics²³ at
417 multiple P value thresholds (from 0.005 to 0.5 at intervals of 0.005, and 1), with higher P value
418 thresholds incorporating larger number of independent SNPs. After quality control of genotype
419 and imaging data, PRSs were generated for 25,861 participants on UK Biobank genotyping
420 data. SNPs were pruned and clumped with a cutoff $r^2 \geq 0.1$ within a 250 kb window. The
421 primary GWAS datasets used for calculating the PRS were listed in Supplementary Table 9.
422 All calculations were conducted using PRSice v2.3.5⁵⁵. Enhanced PRS from UK Biobank
423 Genomics for multiple diseases were also tested. Detailed instructions for calculating enhanced
424 PRS in UK Biobank can be found in ⁵⁶. Comparisons of neuropsychiatric disorders were
425 conducted among participants with different brain aging patterns using t test with FDR
426 correction. All statistical tests were two-sided.

427

428 **Genome Wide Association Study to identify SNPs associated with brain aging patterns**

429 We performed Genome-wide association studies (GWAS) on individual deviations of total
430 GMV relative to the population average at 60 years using PLINK 2.0⁵⁷. Variants with missing
431 call rates exceeding 5%, minor allele frequency below 0.5% and imputation INFO score less
432 than 0.8 were filtered out after the genotyping quality control for UK Biobank Imputation V3
433 dataset. Among the 337,138 unrelated "white British" participants of European ancestry
434 included in our study, 25,861 with recent UK ancestry and accepted genotyping and imaging
435 quality control were included in the GWAS. The analyses were further adjusted for age, age2,
436 sex, assessment center, handedness, ethnic, ICV, and the first 10 genetic principal components.
437 Genome-wide significant SNPs ($P < 5 \times 10^{-8}$) obtained from the GWAS were clumped by
438 linkage disequilibrium (LD) ($r^2 < 0.1$ within a 250 kb window) using UKB release2b White
439 British as the reference panel. We subsequently performed gene-based annotation in FUMA⁵⁸
440 using genome-wide significant SNPs and SNPs in close LD ($r^2 \geq 0.1$) using Annotate Variation
441 (ANNOVAR) on Ensemble v102 genes⁵⁹.

442

443 **Mirroring patterns between brain aging and brain development** To validate the “last in,
444 first out” mirroring hypothesis, we evaluated the structural association between brain

445 development and brain aging. Longitudinal neuroimaging data from 1,529 adolescents in the
446 IMGAEN cohort and 3,908 mid-to-late adulthood in the UK Biobank cohort were analyzed.
447 Annual percentage volume change (APC) for each ROI was calculated among individuals with
448 at least 2 structural MRI scans by subtracting the baseline GMV from follow-up GMV and
449 dividing by the number of years between baseline and follow-up visits. Region-specific APC
450 was regressed on age using smoothing spline with cross validated degree of freedom. Estimated
451 APC for each ROI was obtained at age 15y for adolescents and at age 55y (early aging) and
452 75y (late aging) for participants in UK Biobank. Region-specific APC during adolescence (or
453 mid-to-late adulthood) was then standardized across all cortical regions to create the brain
454 development (or aging) map. Finally, the brain development map and brain aging map were
455 compared to assess the mirroring pattern for each ROI in the overall population and across
456 different aging subgroups.

457

458 **Gene Expression Analysis** The Allen Human Brain Atlas (AHBA) dataset
459 (<http://human.brain-map.org>), which comprises gene expression measurements in six
460 postmortem adults (age 24–57y) across 83 parcellated brain regions^{60,61}, were used to identify
461 gene expressions significantly associated with structural brain development and aging. The
462 expression profiles of 15,633 genes were averaged across donors to form a $83 \times 15,633$
463 transcriptional matrix and partial least squares (PLS) regression was adopted for analyzing the
464 association between regional change rate of gray matter volume and gene expression profiles.
465 Specifically, estimated regional APC at 15 (obtained from IMAGEN cohort) and 55 years old
466 (obtained from UK Biobank) were regressed on the high-dimensional gene expression profiles
467 upon regularization. Associations between the first PLS component and estimated APC during
468 brain development and brain aging were tested by spatial permutation analysis (10,000 times)⁶².
469 Additionally, gene expression profiles of genes mapped to GWAS significant SNP were
470 extracted from AHBA. The association between gene expression profiles of mapped genes and
471 estimated APC during brain development and aging was also tested by spatial permutation
472 analysis. Statistical significance of each gene's contribution to the first PLS component was
473 tested with standard error calculated using bootstrap^{63–65}, and genes significantly associated

474 with delayed brain development and accelerated brain aging were selected. Enrichment of
475 Kyoto Encyclopedia of Genes and Genomes (KEGG) pathways and gene ontology (GO) of
476 biological processes for these selected genes were analyzed using R package clusterProfiler⁶⁶.
477 All statistical significances were corrected for multiple testing using FDR.

478

479 **Data availability**

480 All the UK Biobank data used in the study are available at <https://www.ukbiobank.ac.uk>. The IMAGEN
481 project data are available at <https://imagen-project.org>. GWAS summary statistics used to calculate the
482 PRS are available in the Supplementary Tables 9. Human gene expression data are available in the Allen
483 Human Brain Atlas dataset: <https://human.brainmap.org>.

484

485 **Code availability**

486 R version 4.2.0 was used to perform statistical analyses. FreeSurfer version 6.0 was used to process
487 neuroimaging data. lme4 1.1 in R version 4.2.0 was used to perform longitudinal data analyses. PRSice
488 version 2.3.5 (<https://choishingwan.github.io/PRSice/>) was used to calculate the PRS. PLINK 2.0
489 (www.cog-genomics.org/plink/2.0/) and FUMA version 1.5.6 (<https://fuma.ctglab.nl/>) were used to
490 perform genome-wide association analysis, and ANNOVAR was used to perform gene-based annotation.
491 AHBA microarray expression data were processed using abagen toolbox version 0.1.3
492 (<https://doi.org/10.5281/zenodo.5129257>). The rotate_parcellation code used to perform a spatial
493 permutation test of a parcellated cortical map: https://github.com/frantisekvasa/rotate_parcellation. Code
494 for PLS analysis and bootstrapping to estimate PLS weights are available at
495 https://github.com/KirstieJane/NSPN_WhitakerVertes_PNAS2016/tree/master/SCRIPTS. clusterProfiler
496 4.6 in R version 4.2.0 was used to analyze gene-set enrichment.

497 **References**

- 498 1. Fjell, A. M. & Walhovd, K. B. Structural brain changes in aging: courses, causes and
499 cognitive consequences. *Reviews in the Neurosciences* **21**, 187–222 (2010).
- 500 2. Shaw, P. *et al.* Neurodevelopmental trajectories of the human cerebral cortex. *Journal of*
501 *neuroscience* **28**, 3586–3594 (2008).
- 502 3. Elliott, M. L. *et al.* Brain-age in midlife is associated with accelerated biological aging
503 and cognitive decline in a longitudinal birth cohort. *Molecular psychiatry* **26**, 3829–3838
504 (2021).
- 505 4. Mattson, M. P. & Arumugam, T. V. Hallmarks of brain aging: adaptive and pathological
506 modification by metabolic states. *Cell metabolism* **27**, 1176–1199 (2018).
- 507 5. Park, D. C. & Reuter-Lorenz, P. The adaptive brain: aging and neurocognitive
508 scaffolding. *Annual review of psychology* **60**, 173–196 (2009).
- 509 6. Mariani, E., Polidori, M., Cherubini, A. & Mecocci, P. Oxidative stress in brain aging,
510 neurodegenerative and vascular diseases: an overview. *Journal of Chromatography B* **827**,
511 65–75 (2005).
- 512 7. Kaufmann, T. *et al.* Common brain disorders are associated with heritable patterns of
513 apparent aging of the brain. *Nature neuroscience* **22**, 1617–1623 (2019).
- 514 8. Raz, N., Ghisletta, P., Rodrigue, K. M., Kennedy, K. M. & Lindenberger, U. Trajectories
515 of brain aging in middle-aged and older adults: regional and individual differences.
516 *Neuroimage* **51**, 501–511 (2010).
- 517 9. Raz, N. & Rodrigue, K. M. Differential aging of the brain: patterns, cognitive correlates
518 and modifiers. *Neuroscience & Biobehavioral Reviews* **30**, 730–748 (2006).
- 519 10. Courchesne, E. *et al.* Normal brain development and aging: quantitative analysis at in
520 vivo MR imaging in healthy volunteers. *Radiology* **216**, 672–682 (2000).
- 521 11. McGinnis, S. M., Brickhouse, M., Pascual, B. & Dickerson, B. C. Age-related changes in
522 the thickness of cortical zones in humans. *Brain topography* **24**, 279–291 (2011).
- 523 12. Tamnes, C. K. *et al.* Brain development and aging: overlapping and unique patterns of
524 change. *Neuroimage* **68**, 63–74 (2013).
- 525 13. Douaud, G. *et al.* A common brain network links development, aging, and vulnerability
526 to disease. *Proc. Natl. Acad. Sci. U.S.A.* **111**, 17648–17653 (2014).
- 527 14. Suzuki, H. *et al.* Associations of regional brain structural differences with aging,
528 modifiable risk factors for dementia, and cognitive performance. *JAMA network open* **2**,
529 e1917257–e1917257 (2019).
- 530 15. Fjell, A. M. *et al.* Development and aging of cortical thickness correspond to genetic
531 organization patterns. *Proceedings of the National Academy of Sciences* **112**, 15462–15467
532 (2015).
- 533 16. Nyberg, L. *et al.* Individual differences in brain aging: heterogeneity in cortico-
534 hippocampal but not caudate atrophy rates. *Cerebral Cortex* **33**, 5075–5081 (2023).
- 535 17. Alexander-Bloch, A., Giedd, J. N. & Bullmore, E. Imaging structural co-variance
536 between human brain regions. *Nature Reviews Neuroscience* **14**, 322–336 (2013).
- 537 18. Whitwell, J. L. *et al.* Distinct anatomical subtypes of the behavioural variant of
538 frontotemporal dementia: a cluster analysis study. *Brain* **132**, 2932–2946 (2009).

- 539 19. Levine, M. E. *et al.* An epigenetic biomarker of aging for lifespan and healthspan. *Aging*
540 (*albania NY*) **10**, 573 (2018).
- 541 20. Demanelis, K. *et al.* Determinants of telomere length across human tissues. *Science* **369**,
542 eaaz6876 (2020).
- 543 21. Foster, H. M. *et al.* The effect of socioeconomic deprivation on the association between
544 an extended measurement of unhealthy lifestyle factors and health outcomes: a prospective
545 analysis of the UK Biobank cohort. *The Lancet Public Health* **3**, e576–e585 (2018).
- 546 22. Townsend, P., Phillimore, P. & Beattie, A. *Health and deprivation: inequality and the*
547 *North*. vol. 8 (Taylor & Francis, 2023).
- 548 23. Shi, R. *et al.* Structural neurodevelopment at the individual level - a life-course
549 investigation using ABCD, IMAGEN and UK Biobank data. *medRxiv* 2023–09 (2023).
- 550 24. Smith, S. M. *et al.* An expanded set of genome-wide association studies of brain imaging
551 phenotypes in UK Biobank. *Nature neuroscience* **24**, 737–745 (2021).
- 552 25. Grønborg, M. *et al.* Biomarker Discovery from Pancreatic Cancer Secretome Using a
553 Differential Proteomic Approach* S. *Molecular & Cellular Proteomics* **5**, 157–171 (2006).
- 554 26. Liu, L., Watanabe, N., Akatsu, H. & Nishimura, M. Neuronal expression of ILEI/FAM3C
555 and its reduction in Alzheimer’s disease. *Neuroscience* **330**, 236–246 (2016).
- 556 27. Smith, S. M. *et al.* Brain aging comprises many modes of structural and functional
557 change with distinct genetic and biophysical associations. *elife* **9**, e52677 (2020).
- 558 28. Estrada, K. *et al.* Genome-wide meta-analysis identifies 56 bone mineral density loci and
559 reveals 14 loci associated with risk of fracture. *Nature genetics* **44**, 491–501 (2012).
- 560 29. Bohl, J., Brimer, N., Lyons, C. & Pol, S. B. V. The stardust family protein MPP7 forms a
561 tripartite complex with LIN7 and DLG1 that regulates the stability and localization of DLG1
562 to cell junctions. *Journal of Biological Chemistry* **282**, 9392–9400 (2007).
- 563 30. Kaech, S. M., Whitfield, C. W. & Kim, S. K. The LIN-2/LIN-7/LIN-10 complex
564 mediates basolateral membrane localization of the C. elegans EGF receptor LET-23 in vulval
565 epithelial cells. *Cell* **94**, 761–771 (1998).
- 566 31. Lanktree, M. *et al.* Association study of brain-derived neurotrophic factor (BDNF) and
567 LIN-7 homolog (LIN-7) genes with adult attention-deficit/hyperactivity disorder. *American*
568 *Journal of Medical Genetics Part B: Neuropsychiatric Genetics* **147**, 945–951 (2008).
- 569 32. Habes, M. *et al.* Disentangling heterogeneity in Alzheimer’s disease and related
570 dementias using data-driven methods. *Biological psychiatry* **88**, 70–82 (2020).
- 571 33. Berg, D. *et al.* Prodromal Parkinson disease subtypes—key to understanding
572 heterogeneity. *Nature Reviews Neurology* **17**, 349–361 (2021).
- 573 34. Ferreira, D., Nordberg, A. & Westman, E. Biological subtypes of Alzheimer disease: A
574 systematic review and meta-analysis. *Neurology* **94**, 436–448 (2020).
- 575 35. Feczko, E. *et al.* The heterogeneity problem: approaches to identify psychiatric subtypes.
576 *Trends in cognitive sciences* **23**, 584–601 (2019).
- 577 36. Poulakis, K. *et al.* Multi-cohort and longitudinal Bayesian clustering study of stage and
578 subtype in Alzheimer’s disease. *Nature communications* **13**, 4566 (2022).
- 579 37. Bogousslavsky, J., Miklossy, J., Deruaz, J.-P., Assal, G. & Regli, F. Lingual and fusiform
580 gyri in visual processing: a clinico-pathologic study of superior altitudinal hemianopia.
581 *Journal of Neurology, Neurosurgery & Psychiatry* **50**, 607–614 (1987).

- 582 38. Epstein, R., Harris, A., Stanley, D. & Kanwisher, N. The parahippocampal place area:
583 recognition, navigation, or encoding? *Neuron* **23**, 115–125 (1999).
- 584 39. Mechelli, A., Humphreys, G. W., Mayall, K., Olson, A. & Price, C. J. Differential effects
585 of word length and visual contrast in the fusiform and lingual gyri during. *Proceedings of the*
586 *Royal Society of London. Series B: Biological Sciences* **267**, 1909–1913 (2000).
- 587 40. Chételat, G. *et al.* Using voxel-based morphometry to map the structural changes
588 associated with rapid conversion in MCI: a longitudinal MRI study. *Neuroimage* **27**, 934–946
589 (2005).
- 590 41. Yao, Z. *et al.* Abnormal cortical networks in mild cognitive impairment and Alzheimer’s
591 disease. *PLoS computational biology* **6**, e1001006 (2010).
- 592 42. Tian, Y. E. *et al.* Heterogeneous aging across multiple organ systems and prediction of
593 chronic disease and mortality. *Nature Medicine* **29**, 1221–1231 (2023).
- 594 43. Aljondi, R., Szoek, C., Steward, C., Yates, P. & Desmond, P. A decade of changes in
595 brain volume and cognition. *Brain imaging and behavior* **13**, 554–563 (2019).
- 596 44. Raz, N. Aging of the brain and its impact on cognitive performance: Integration of
597 structural and functional findings. (2000).
- 598 45. Honea, R., Crow, T. J., Passingham, D. & Mackay, C. E. Regional deficits in brain
599 volume in schizophrenia: a meta-analysis of voxel-based morphometry studies. *American*
600 *Journal of Psychiatry* **162**, 2233–2245 (2005).
- 601 46. Schultz, C. C. *et al.* Increased parahippocampal and lingual gyrification in first-episode
602 schizophrenia. *Schizophrenia Research* **123**, 137–144 (2010).
- 603 47. Hoogman, M. *et al.* Brain imaging of the cortex in ADHD: a coordinated analysis of
604 large-scale clinical and population-based samples. *American Journal of Psychiatry* **176**, 531–
605 542 (2019).
- 606 48. Glahn, D. C. *et al.* Genetic basis of neurocognitive decline and reduced white-matter
607 integrity in normal human brain aging. *Proceedings of the National Academy of Sciences* **110**,
608 19006–19011 (2013).
- 609 49. Brouwer, R. M. *et al.* Genetic variants associated with longitudinal changes in brain
610 structure across the lifespan. *Nature neuroscience* **25**, 421–432 (2022).
- 611 50. Zheng, H.-F. *et al.* Whole-genome sequencing identifies EN1 as a determinant of bone
612 density and fracture. *Nature* **526**, 112–117 (2015).
- 613 51. Ghafouri-Fard, S., Khoshbakht, T., Taheri, M. & Ghanbari, M. A concise review on the
614 role of BDNF-AS in human disorders. *Biomedicine & Pharmacotherapy* **142**, 112051 (2021).
- 615 52. Desikan, R. S. *et al.* An automated labeling system for subdividing the human cerebral
616 cortex on MRI scans into gyral based regions of interest. *Neuroimage* **31**, 968–980 (2006).
- 617 53. Fischl, B. *et al.* Whole brain segmentation: automated labeling of neuroanatomical
618 structures in the human brain. *Neuron* **33**, 341–355 (2002).
- 619 54. Codd, V. *et al.* Polygenic basis and biomedical consequences of telomere length
620 variation. *Nature genetics* **53**, 1425–1433 (2021).
- 621 55. Choi, S. W. & O’Reilly, P. F. PRSice-2: Polygenic Risk Score software for biobank-scale
622 data. *Gigascience* **8**, giz082 (2019).
- 623 56. Thompson, D. J. *et al.* UK Biobank release and systematic evaluation of optimised
624 polygenic risk scores for 53 diseases and quantitative traits. *MedRxiv* 2022–06 (2022).

- 625 57. Chang, C. C. *et al.* Second-generation PLINK: rising to the challenge of larger and richer
626 datasets. *Gigascience* **4**, s13742-015 (2015).
- 627 58. Watanabe, K., Taskesen, E., Van Bochoven, A. & Posthuma, D. Functional mapping and
628 annotation of genetic associations with FUMA. *Nature communications* **8**, 1826 (2017).
- 629 59. Wang, K., Li, M. & Hakonarson, H. ANNOVAR: functional annotation of genetic
630 variants from high-throughput sequencing data. *Nucleic acids research* **38**, e164–e164
631 (2010).
- 632 60. Hawrylycz, M. J. *et al.* An anatomically comprehensive atlas of the adult human brain
633 transcriptome. *Nature* **489**, 391–399 (2012).
- 634 61. Markello, R. D. *et al.* Standardizing workflows in imaging transcriptomics with the
635 abagen toolbox. *elife* **10**, e72129 (2021).
- 636 62. Váša, F. *et al.* Adolescent Tuning of Association Cortex in Human Structural Brain
637 Networks. *Cerebral Cortex* **28**, 281–294 (2018).
- 638 63. Li, J. *et al.* Cortical structural differences in major depressive disorder correlate with cell
639 type-specific transcriptional signatures. *Nature communications* **12**, 1647 (2021).
- 640 64. Morgan, S. E. *et al.* Cortical patterning of abnormal morphometric similarity in
641 psychosis is associated with brain expression of schizophrenia-related genes. *Proceedings of*
642 *the National Academy of Sciences* **116**, 9604–9609 (2019).
- 643 65. Romero-Garcia, R. *et al.* Schizotypy-related magnetization of cortex in healthy
644 adolescence is colocated with expression of schizophrenia-related genes. *Biological*
645 *psychiatry* **88**, 248–259 (2020).
- 646 66. Yu, G., Wang, L.-G., Han, Y. & He, Q.-Y. clusterProfiler: an R package for comparing
647 biological themes among gene clusters. *Omics: a journal of integrative biology* **16**, 284–287
648 (2012).
- 649

650 **Acknowledgements**

651 This research used the UK Biobank Resource under application number 19542. We thank all
652 participants and researchers from the UK Biobank. We thank the IMAGEN Consortium for
653 providing the discover data. This work received support from the following sources: National
654 Key R&D Program of China (No.2019YFA0709502), National Key R&D Program of China
655 (No.2018YFC1312904), Shanghai Municipal Science and Technology Major Project
656 (No.2018SHZDZX01), ZJ Lab, and Shanghai Center for Brain Science and Brain-Inspired
657 Technology, the 111 Project (No.B18015), the European Union-funded FP6 Integrated
658 Project IMAGEN (Reinforcement-related behaviour in normal brain function and
659 psychopathology) (LSHM-CT- 2007-037286), the Horizon 2020 funded ERC Advanced
660 Grant ‘STRATIFY’ (Brain network based stratification of reinforcement-related disorders)
661 (695313), Human Brain Project (HBP SGA 2, 785907, and HBP SGA 3, 945539), the
662 Medical Research Council Grant ‘c-VEDA’ (Consortium on Vulnerability to Externalizing
663 Disorders and Addictions) (MR/N000390/1), the National Institute of Health (NIH)
664 (R01DA049238, A decentralized macro and micro gene-by-environment interaction analysis
665 of substance use behavior and its brain biomarkers), the National Institute for Health
666 Research (NIHR) Biomedical Research Centre at South London and Maudsley NHS
667 Foundation Trust and King’s College London, the Bundesministerium für Bildung und
668 Forschung (BMBF grants 01GS08152; 01EV0711; Forschungsnetz AERIAL 01EE1406A,
669 01EE1406B; Forschungsnetz IMAC-Mind 01GL1745B), the Deutsche
670 Forschungsgemeinschaft (DFG grants SM 80/7-2, SFB 940, TRR 265, NE 1383/14-1), the
671 Medical Research Foundation and Medical Research Council (grants MR/R00465X/1 and
672 MR/S020306/1), the National Institutes of Health (NIH) funded ENIGMA (grants
673 5U54EB020403-05 and 1R56AG058854-01), NSFC grant 82150710554 and European
674 Union funded project ‘environMENTAL’, grant no: 101057429. Further support was
675 provided by grants from: - the ANR (ANR-12-SAMA-0004, AAPG2019 - GeBra), the Eranet
676 Neuron (AF12-NEUR0008-01 - WM2NA; and ANR-18-NEUR00002-01 - ADORe), the
677 Fondation de France (00081242), the Fondation pour la Recherche Médicale
678 (DPA20140629802), the Mission Interministérielle de Lutte-contre-les-Drogues-et-les-
679 Conduites-Addictives (MILDECA), the Assistance-Publique-Hôpitaux-de-Paris and
680 INSERM (interface grant), Paris Sud University IDEX 2012, the Fondation de l’Avenir
681 (grant AP-RM-17-013), the Fédération pour la Recherche sur le Cerveau; the National
682 Institutes of Health, Science Foundation Ireland (16/ERC/CD/3797), U.S.A. (Axon,
683 Testosterone and Mental Health during Adolescence; RO1 MH085772-01A1) and by NIH
684 Consortium grant U54 EB020403, supported by a cross-NIH alliance that funds Big Data to
685 Knowledge Centres of Excellence. The funders had no role in study design, data collection
686 and analysis, decision to publish or preparation of the manuscript.

687

688 **Competing interests**

689 Dr Banaschewski served in an advisory or consultancy role for eye level, Infectopharm,
690 Lundbeck, Medice, Neurim Pharmaceuticals, Oberberg GmbH, Roche, and Takeda. He
691 received conference support or speaker’s fee by Janssen, Medice and Takeda. He received

692 royalties from Hogrefe, Kohlhammer, CIP Medien, Oxford University Press; the present
693 work is unrelated to these relationships. Dr Poustka served in an advisory or consultancy role
694 for Roche and Viforpharm and received speaker's fee by Shire. She received royalties from
695 Hogrefe, Kohlhammer and Schattauer. The present work is unrelated to the above grants and
696 relationships. The other authors report no biomedical financial interests or potential conflicts
697 of interest.

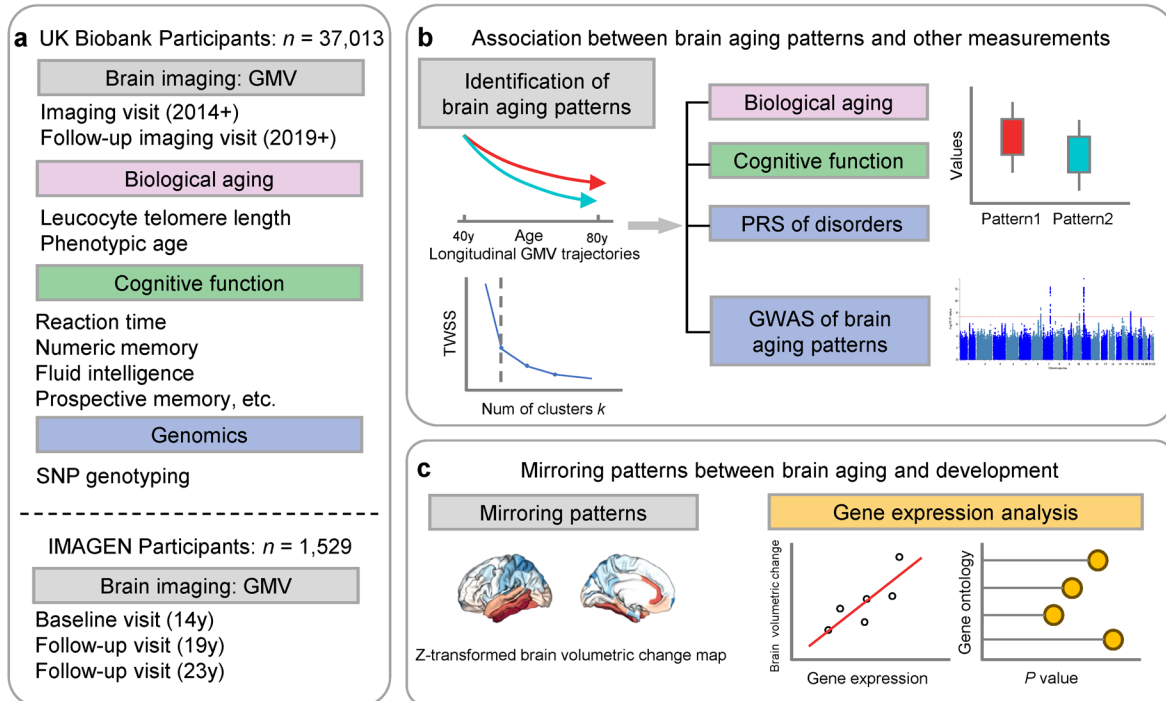


Fig. 1 Overview of the study workflow. **a**, Population cohorts (UK Biobank and IMAGEN) and data sources (brain imaging, biological aging biomarkers, cognitive functions, genomic data) involved in this study. **b**, Brain aging patterns were identified using longitudinal trajectories of the whole brain GMV, and associations between brain aging patterns and other measurements (biological aging, cognitive functions and PRS of major neuropsychiatric disorders) were investigated. **c**, Mirroring patterns between brain aging and brain development was investigated using z-transformed brain volumetric change map and gene expression analysis.

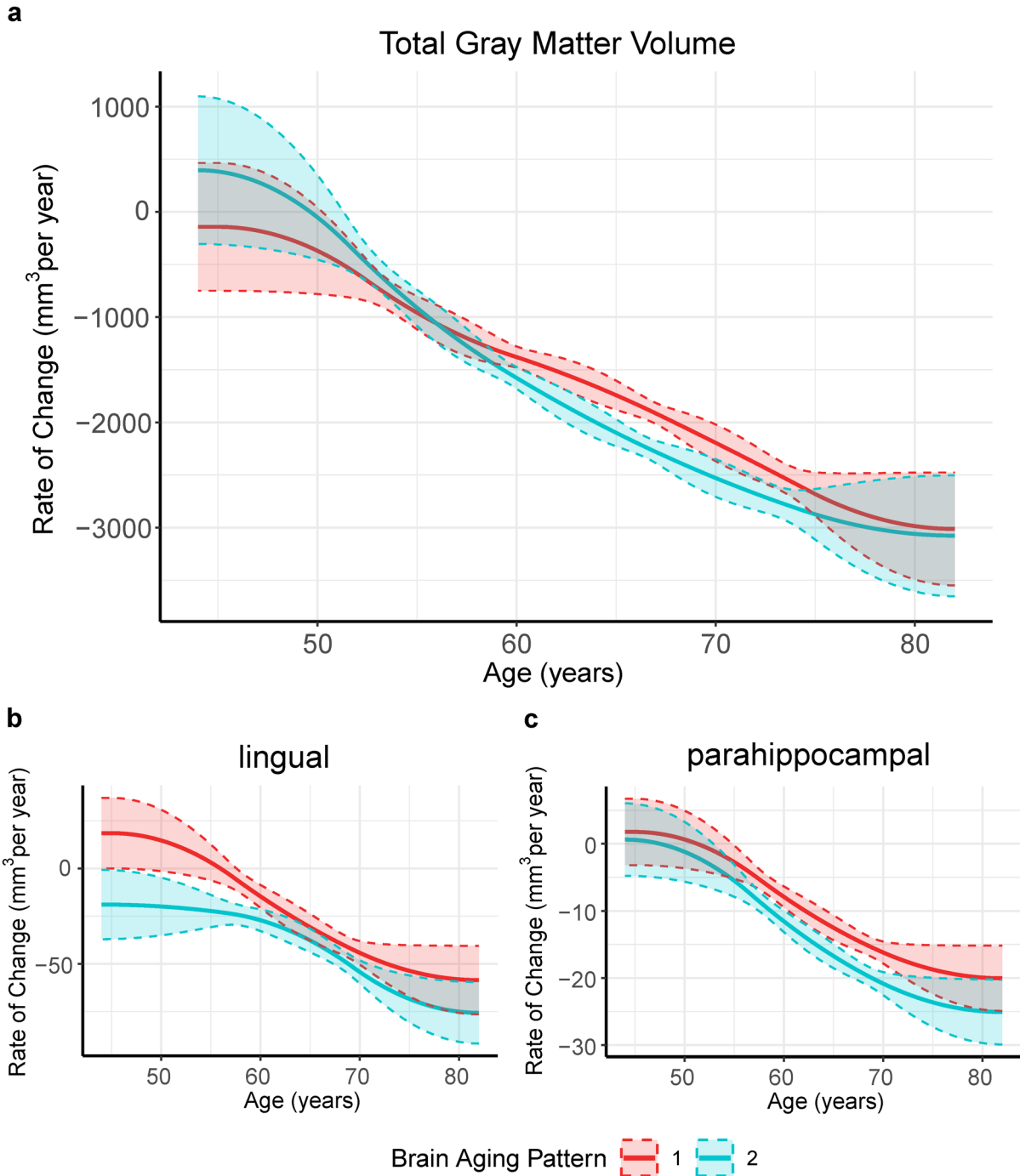


Fig. 2 Global (a) and selected regional (b, c) cortical gray matter volume rate of change among participants with brain aging patterns 1 (red) and 2 (blue). Rates of volumetric change for total gray matter and each ROI were estimated using GAMM, which incorporates both cross-sectional between-subject variation and longitudinal within-subject variation from 40,921 observations and 37,013 participants. Covariates include sex, assessment center, handedness, ethnic, and ICV. Shaded areas around the fit line denotes 95% CI.

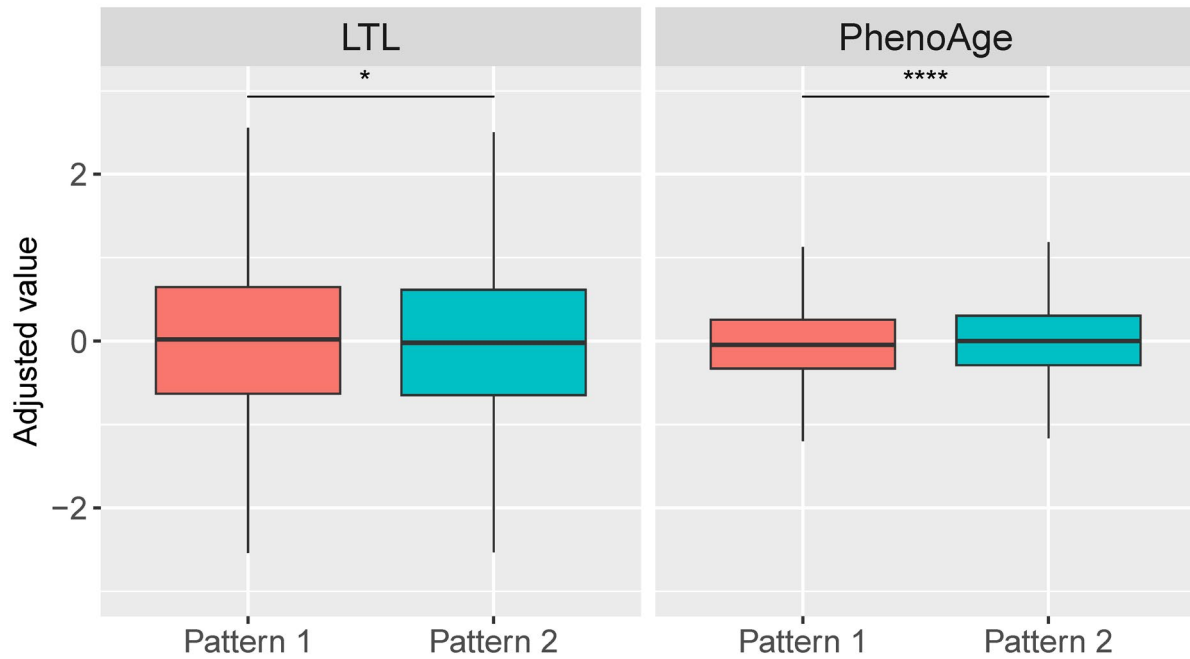


Fig. 3 Distributions of biological aging biomarkers (leucocyte telomere length (LTL) and PhenoAge) among participants with brain aging patterns 1 and 2. Boxes represent the interquartile range (IQR), lines within the boxes indicate the median, and whiskers indicate potential outliers (values outside of the 1.5 IQR range). Two-sided P values were obtained by comparing LTL or PhenoAge¹⁹ between brain aging patterns using unadjusted multivariate linear regression models. Results remained significant when adjusting for sex, age, ethnic, BMI, smoking status and alcohol intake frequency in the LTL model²⁰ and sex, age, ethnic, BMI, smoking status, alcohol frequency and education years in PhenoAge model. Stars indicate statistical significance after Bonferroni correction. *****: $p \leq 0.0001$, *: $p \leq 0.05$.

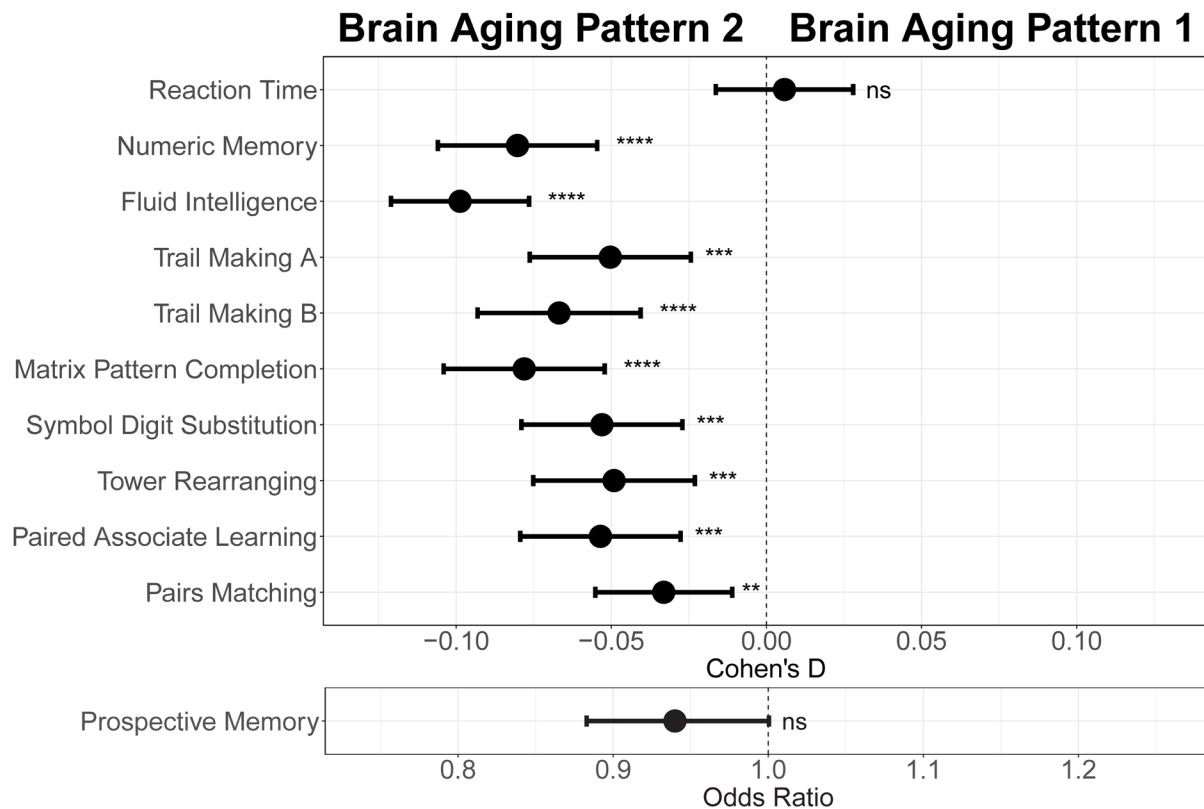


Fig. 4 Effect size (Cohen's D or odds ratio) for comparing the cognitive functions between participants with brain aging patterns 1 and 2. Results were adjusted such that negative Cohen's D and Odds Ratio less than 1 indicate worse cognitive performances in brain aging pattern 2 compared to pattern 1. Width of the lines extending from the center point represent 95% confidence interval. Two-sided P values were obtained using both unadjusted and adjusted (for sex, age, and TDI, education and income) multivariate regression models. Stars indicate statistical significance after FDR correction for 11 comparisons. ****: $p \leq 0.0001$, ***: $p \leq 0.001$, **: $p \leq 0.01$, ns: $p > 0.05$.

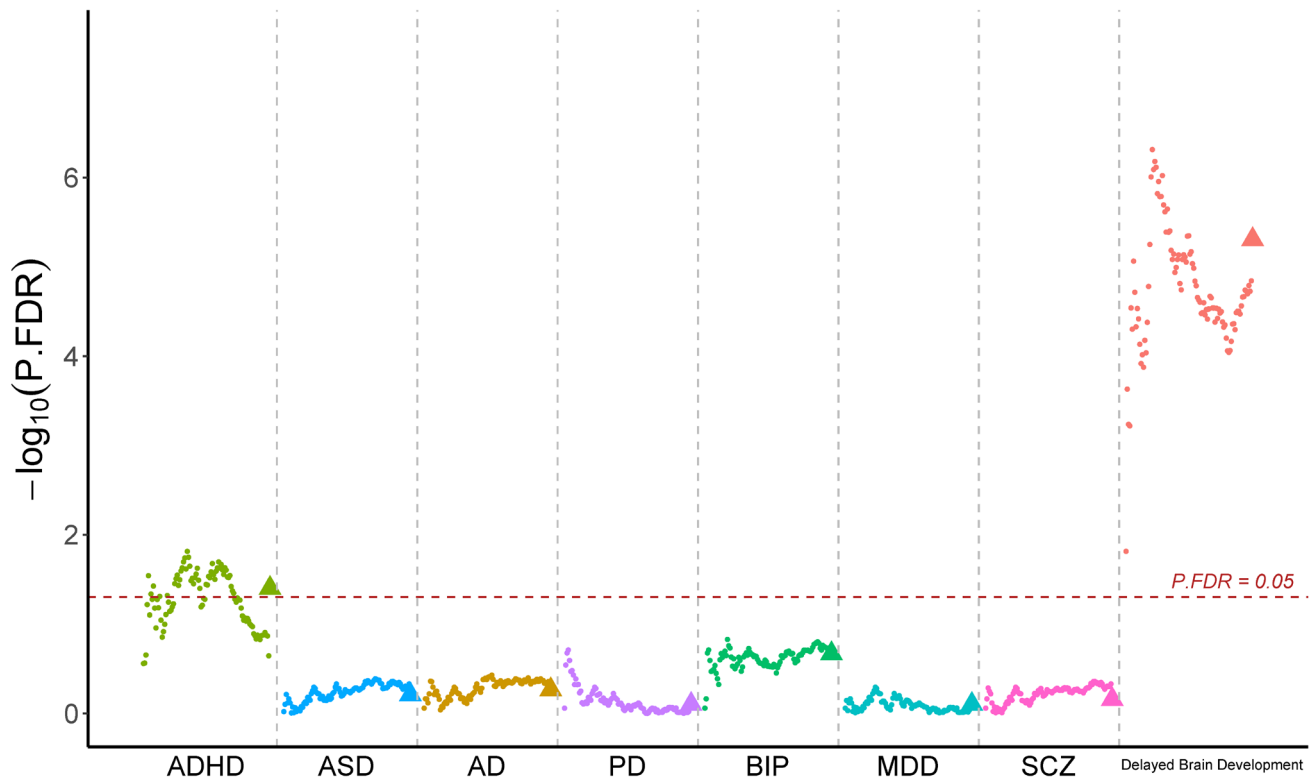


Fig. 5 Participants with accelerated brain aging (brain aging pattern 2) had significantly increased genetic liability to ADHD and delayed brain development. Polygenic risk score (PRS) for ADHD, ASD, AD, PD, BIP, MDD, SCZ and delayed brain development (unpublished GWAS) were calculated at different p-value thresholds from 0.005 to 0.5 at an interval of 0.005. Vertical axis represents negative logarithm of P values comparing PRS in brain aging pattern 2 relative to pattern 1. Red horizontal dashed line indicates FDR corrected P value of 0.05. Colors represent traits and dots within the same color represent different p value thresholds. The trigonometric symbol indicates the average PRS across all p-value thresholds for the same trait.

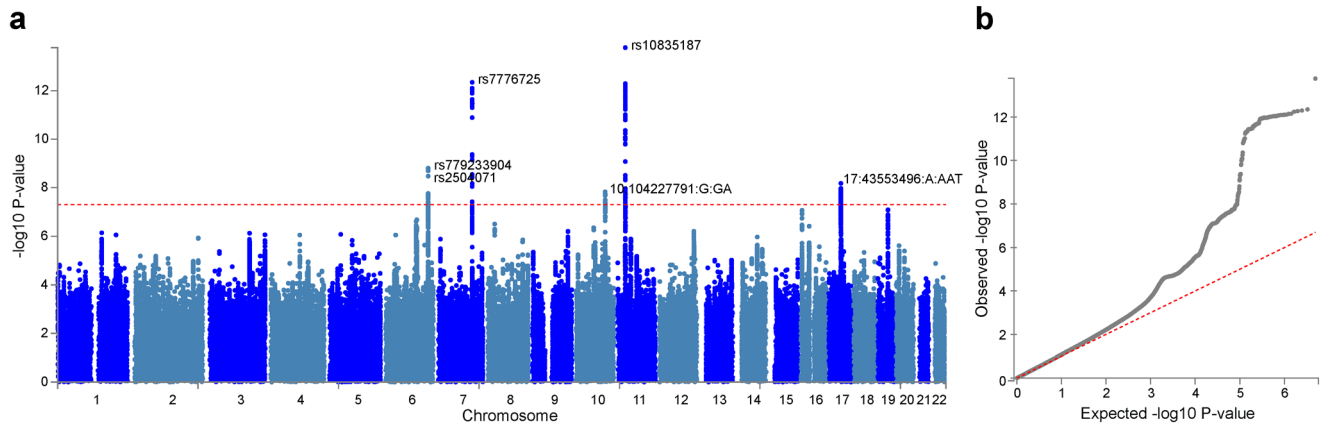


Fig. 6 Genome-wide association study (GWAS) identified 6 independent SNPs associated with accelerated brain aging. Total GMV at 60 years old was estimated for each participant using mixed effect models allowing for individualized baseline GMV and GMV change rate, and was used as the phenotype in the GWAS. **a**, At genome-wide significance level ($P=5e-8$, red dashed line), rs10835187 and rs7776725 loci were identified to be associated with accelerated brain aging. **b**, Quantile–quantile plot showed that the most significant P values deviate from the null, suggesting that results are not unduly inflated.

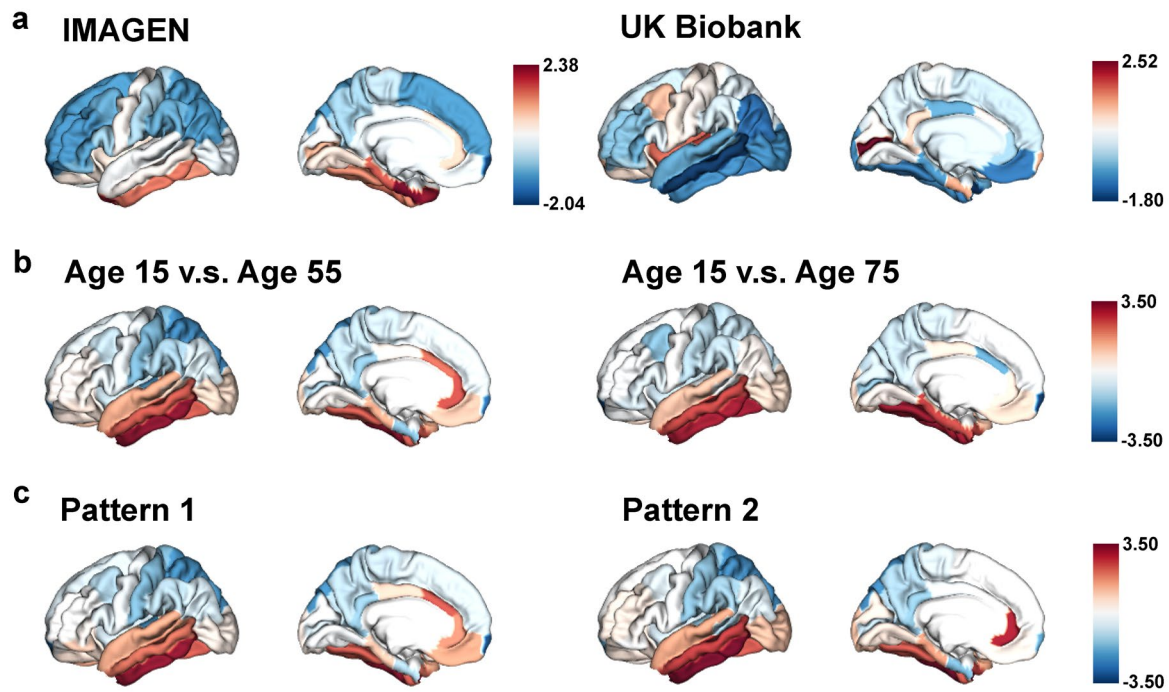


Fig. 7 The “last in, first out” mirroring patterns between brain development and brain aging. **a**, The annual percentage volume change (APC) was calculated for each ROI and standardized across the whole brain in adolescents (IMAGEN, left) and mid-to-late aged adults (UK Biobank, right), respectively. For adolescents, ROIs in red indicate delayed structural brain development, while for mid-to-late aged adults, ROIs in blue indicate accelerated structural brain aging. **b**, Estimated APC in brain development versus early aging (55 years old, left), and versus late aging (75 years old, right). ROIs in red indicate faster GMV decrease during brain aging and slower GMV decrease during brain development, i.e., stronger mirroring effects between brain development and brain aging. **c**, Mirroring patterns between brain development and brain aging were more manifested in participants with accelerated aging (brain aging pattern 2).

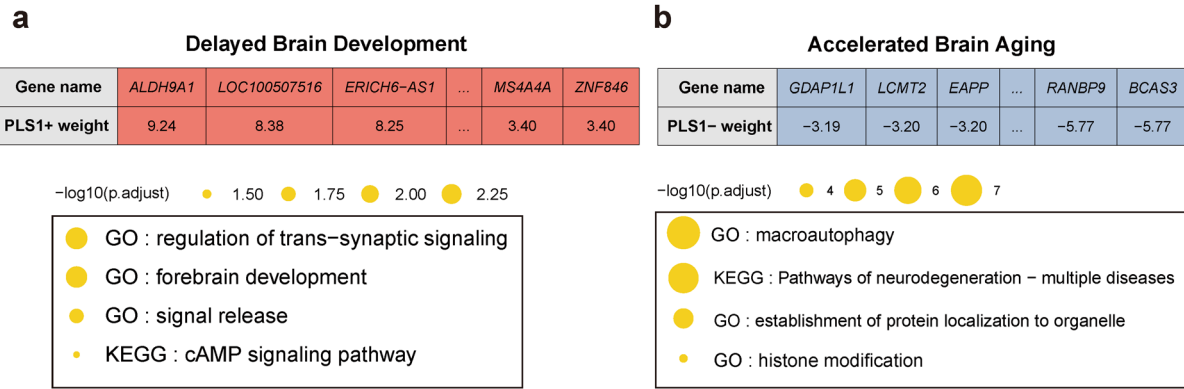


Fig. 8 Functional enrichment of gene transcripts significantly associated with delayed brain development and accelerated brain aging. **a**, 990 genes were spatially correlated with the first PLS component of delayed structural brain development, and were enriched for trans-synaptic signal regulation, forebrain development, signal release and cAMP signaling pathway. **b**, 2,293 genes were spatially correlated the first PLS component of accelerated structural brain aging, and were enriched for macroautophagy, pathways of neurodegeneration, establishment of protein localization to organelle and histone modification. Size of the circle represents number of genes in each term and P values were corrected using FDR for multiple comparisons.